The Astronomical Journal, 160:122 (15pp), 2020 September https://doi.org/10.3847/1538-3881/aba754

Self-consistent Color–Stellar Mass-to-light Ratio Relations for Low Surface Brightness Galaxies

Wei Du[1,2] and Stacy S. McGaugh[2]
[1] Key Laboratory of Optical Astronomy, National Astronomical Observatories, Chinese Academy of Sciences, 20A Datun Road, Chaoyang District, Beijing 100101, People's Republic of China; wdu@nao.cas.cn, wxd165@case.edu
[2] Department of Astronomy, Case Western Reserve University, 10900 Euclid Avenue, Cleveland, OH 44106, USA
Received 2020 March 10; revised 2020 July 9; accepted 2020 July 16; published 2020 August 17

Abstract

The color–stellar mass-to-light ratio relation (CMLR) is a widely accepted tool for estimating the stellar mass (M_*) of a galaxy. However, an individual CMLR tends to give distinct M_* for a same galaxy when it is applied in different bands. Examining five representative CMLRs from the literature, we find that the difference in M_* predicted in different bands from optical to near-infrared by a CMLR is 0.1 $\sim$ 0.3 dex. Based on a sample of low surface brightness galaxies that covers a wide range of color and luminosity, we therefore recalibrated each original CMLR in r, i, z, J, H, and K bands to give internally self-consistent M_* for a same galaxy. The g–r is the primary color indicator in the recalibrated relations, which show little dependence on red (r–z) or near-infrared (J–K) colors. Additionally, the external discrepancies in the originally predicted γ_* by the five independent CMLRs have been greatly reduced after recalibration, especially in the near-infrared bands, implying that the near-infrared luminosities are more robust in predicting γ_*. For each CMLR, the recalibrated relations provided in this work could produce internally self-consistent M_* from divergent photometric bands, and are extensions of the recalibrations from the Johnson–Cousin filter system by the pioneering work of McGaugh & Schombert to the filter system of the Sloan Digital Sky Survey.

Unified Astronomy Thesaurus concepts: Low surface brightness galaxies (940); Galaxy stellar content (621); Photometry (1234); Galaxy properties (615); Scaling relations (2031)

1. Introduction

The stellar mass (M_*) is one of the fundamental physical properties of a galaxy because it traces the star formation and evolution process of the galaxy, and it is crucial for decomposing the contributions from stars and dark matter to the dynamics of a galaxy. The stellar population synthesis (SPS) technique is an efficient way to estimate M_* of a galaxy by fitting the SPS models that rely on the extant stellar evolution theory to galaxy data, either in the form of observed multiband spectral energy distributions (SEDs), spectra, or spectral indices of the galaxy. This fit method requires data of SED or spectra, but not all the galaxies have multiband imaging or spectroscopic data, so that a simple color-based method is more practical for estimating M_* of a galaxy. The pioneering works of Bell & de Jong (2001; hereafter Bdj01) and Bell et al. (2003; hereafter B03) have defined the relations between color and stellar mass-to-light ratio (γ_*) of galaxies in the form of Equation (1),

$$\log \gamma_*^j = a_j + b_j \times \mathrm{color}. \quad (1)$$

The γ_* of a galaxy can be predicted from the color–stellar mass-to-light ratio relation (CMLR), and it can subsequently be multiplied by the galaxy luminosity to yield M_* of the galaxy. The CMLR method requires minimal data and is hence expedient in all applications related to the M_* estimate. In this way, a variety of CMLRs have emerged. A number of these CMLRs are calibrated on model galaxies (e.g., Gallazzi & Bell 2009; Zibetti et al. 2009; hereafter Z09; Into & Portinari 2013; hereafter IP13; Roediger & Courteau 2015; hereafter RC15), and some are calibrated on samples of observed galaxies, such as spiral galaxies (e.g., B03, Portinari et al. 2004; Taylor et al. 2011), dwarf galaxies (e.g., Herrmann et al. 2016), and low surface brightness galaxies (e.g., Du et al. 2020). For galaxies, the CMLR method could recover γ_* from a single color within an accuracy of $\sim$0.1–0.2 dex (Bell & de Jong 2001), and could produce M_* equivalent to those derived from SED fit method on average (Roediger & Courteau 2015; Du et al. 2020).

However, in the aspect of the CMLR-based M_*, McGaugh & Schombert (2014; hereafter MS14) found that the existing CMLR tends to give different M_* for the same galaxy when it is applied in different photometric bands. Based on a sample of disk galaxies, they recalibrated several representative CMLRs in the Johnson–Cousin filter system to ultimately produce internally self-consistent M_* for the same galaxy when it is applied to different bands of V, I, K, and [3.6] bands (with B–V as color indicator). Inspired by MS14, we expect to extend their work from the Johnson–Cousins bands to the Sloan Digital Sky Survey (SDSS) optical bands and near-infrared (NIR) bands in this work, based on a sample of low surface brightness galaxies (LSBGs), by first examining the internal self-consistency of a CMLR in M_* estimates from different bands and then recalibrating the CMLR to be able to give internally self-consistent M_* estimates from different bands for the same galaxy.

We describe the data in Section 2 and introduce the five representative CMLR models in Section 3. We estimated M_* from different bands for the sample by the CMLRs, and internally compared M_* from different bands by each

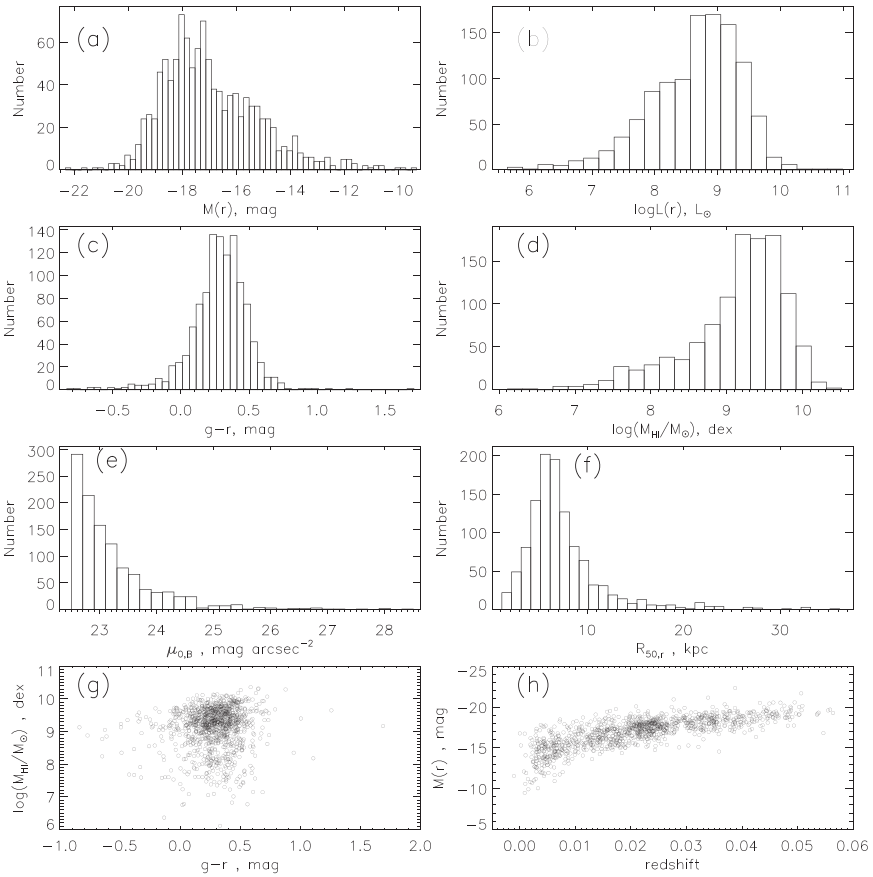

Figure 1. Properties of the LSBG sample. In panels (a)–(f), the distributions of r-band absolute magnitude (M(r)), the r-band luminosity in logarithm (log L(r)), g–r color (g–r), H I mass in logarithm (log $M_{H_I}/M_\odot$), B-band central surface brightness ($\mu_{0,B}$), and effective radius ($R_{50,r}$) are shown, respectively. Panels (g) and (h) show g–r vs. H I mass, and M(r) vs. redshift, respectively.

individual CMLR, and then externally compared M_* predicted by different CMLRs in Section 4. In Section 5 each individual CMLR is recalibrated to be internally self-consistent in M_* estimates for the sample, when it is applied in different bands from optical to NIR. We discuss this in Section 6, including the possible second color term to the recalibrated relations in Section 6.1, the error budget in γ_* predicted by the recalibrated relations in Section 6.2, a comparison between the originally predicted γ_* and those predicted by the recalibrated relations in Section 6.3, and a comparison between recalibrated relations in this work and those by MS14 in Section 6.4. A summary and conclusion are given in Section 7. Throughout the work, the magnitude is in the AB magnitude system, and the galaxy distance we used to calculate the absolute magnitude and luminosity is taken directly from the Arecibo Legacy Fast ALFA Survey (ALFALFA) catalog of Haynes et al. (2018), which adopts a Hubble constant of $H_0 = 70\,\mathrm{km\,s^{-1}\,Mpc^{-1}}$.

2. Data

2.1. LSBG Sample

Because LSBGs are typically gas rich, we have defined a sample of LSBGs from a survey combination of α.40 H I (Haynes et al. 2011) and SDSS DR7 photometric surveys (Abazajian et al. 2009). The selection of this sample has been reported in detail in Du et al. (2015) and Du et al. (2019). This sample includes 1129 LSBGs whose B-band central surface brightnesses ($\mu_{0,B}$) are fainter than 22.5 mag arcsec^{-2} ($\mu_{0,\,B} > 22.5$), and the parameter space of the sample extends the paramaeter space covered by previous LSBG samples to fainter luminosity, lower H I gas mass, and bluer color (Figure 1). In color, the full range of this sample is $-0.8 < g - r < 1.7$ (the peak is at 0.28, and it has a 1σ scatter of 0.21), with 95.4% within $-0.14 < g - r < 0.70$ and 68.3% within $0.07 < g - r < 0.49$. In absolute magnitude, the full range of the sample spans over 10 mag, with 95.4% within $-13 < M_r < -21$ mag and 68.3% within $-15 < M_r < -19$ mag. In terms of luminosity, it is composed of dwarf ($M_B \geqslant -17.0$ mag; 54% of the sample), moderate-luminosity ($-19.0 < M_B < -17.0$ mag; 43%), and giant galaxies ($M_B \leqslant -19.0$ mag; 3%). In terms of morphology, it is dominated by late-type spiral and irregular galaxies (Sd/Sm/Im; 84.1% of the sample), then the early- and middle-type spiral galaxies (Sa/Sab/Sb/Sbc/Sc/Scd;13.4%), and finally the early-type galaxies (E/S0; 0.2%)(Du et al. 2019). In this work, we intend to recalibrate several literature CMLRs (Section 3) based on this sample of LSBGs.

2.2. Photometry

The optical images (*griz* bands) of the sample were downloaded from SDSS DR7 (Abazajian et al. 2009), and the NIR images (*JHK* bands) were obtained from UKIDSS (Lawrence et al. 2007). For each image, we subtracted the sky background, excluded the bright disturbing objects around the target galaxy, and replaced the masked pixels with the mean value of the surrounding background pixels. The magnitudes of the target galaxy were then measured in these bands in Du et al. (2020) with SExtractor (Bertin & Arnouts 1996) in the

Table 1
Original CMLRs Based on g–r Color

model	IMF	TP-AGB	a_r	b_r	a_i	b_i	a_z	b_z	a_J	b_J	a_H	b_H	a_K	b_K
B03	"diet" Salpeter	Girardi	−0.306	1.097	−0.222	0.864	−0.223	0.689	−0.172	0.444	−0.189	0.266	−0.209	0.197
IP13	Kroupa	Marigo	−0.663	1.530	−0.633	1.370	−0.665	1.292	−0.732	1.139	−0.880	1.128	−0.945	1.153
Z09	Chabrier	Marigo	−0.840	1.654	−0.845	1.481	−0.914	1.382	−1.007	1.225	−1.147	1.144	−1.257	1.119
RC15(BC03)	Chabrier	Girardi	−0.792	1.629	−0.771	1.438	−0.796	1.306	⋯	⋯	−0.920	0.980	⋯	⋯
RC15(FSPS)	Chabrier	Marigo	−0.647	1.497	−0.602	1.281	−0.583	1.102	⋯	⋯	−0.605	0.672	⋯	⋯

Note. Stellar mass-to-light ratios (γ_*) in SDSS r, i, z and NIR J, H, K bands are given by the CMLRs of Bell et al. (2003, B03), Into & Portinari (2013, IP13), Zibetti et al. (2009, Z09), Roediger & Courteau (2015) based on BC03 model (RC15(BC03)), and Roediger & Courteau (2015) based on FSPS model (RC15(FSPS) in the formula of $\log \gamma_*^j = a_j + b_j \times (g - r)$. For reference, the initial mass function (IMF) and the TP-AGB prescription adopted by each CMLR model are also given. For the IMF, "Kroupa" denotes the Kroupa (1998) IMF, and "Chabrier" denotes the Chabrier (2003) IMF. For TP-AGB, the "Girardi" denotes the simplified TP-AGB prescriptions (e.g., Girardi & Bertelli 1998; Girardi et al. 2000, 2002), while "Marigo" denotes the relatively new TP-AGB prescriptions (e.g., Marigo & Girardi 2007; Marigo et al. 2008), which incorporate a larger number of TP-AGB stars.

dual-image mode, in which the r-band image is regarded as a reference and is used to detect the galaxy source and define the photometric apertures (center, size, and shape). Images of the same galaxy in all other bands are photometrically measured within the same aperture defined in the r band. The measured magnitudes in all the bands are corrected for Galactic extinction using the prescription of Schlafly & Finkbeiner (2011). As LSBGs are poor in dust content, we do not correct the internal extinction to magnitudes. Finally, magnitudes in all the bands were converted into the AB magnitude system. We adopt a distance given in ALFALFA catalog (Haynes et al. 2018) to compute the absolute magnitude and luminosity in each band of *grizJHK*. As the aperture definition for each galaxy does not vary between wavelength bands, this measurement gives internally consistent colors.

3. CMLR Models

In the pioneering work of MS14, the CMLRs of B03, Z09, IP13, and Portinari et al. (2004) (P04) are recalibrated in the *V, I, K*, and [3.6] bands with B–V as the color indicator. In this work, we aim to extend MS14 from Johnson–Cousins filters to SDSS optical and two more NIR filters. In addition to the three CMLRs of B03, Z09, and IP13 studied in MS14, which also provide relations in SDSS bands, two more CMLRs of the RC15 based on the BC03 stellar population model (RC15(BC03)) and the FSPS model (RC15(FSPS)) will be considered.

B03 worked with an empirical relation, while the other relations (Z09, IP13, RC15) are theoretical. B03 based their work on a sample of observed galaxies, which are mostly bright galaxies ($13 \leqslant r \leqslant 17.5$ mag) with high surface brightnesses (HSB; $\mu_r < 21$ mag arcsec^{-2}). Their sample spans the full range of $0.2 < g$–$r < 1.2$, and most galaxies lie within the range of $0.4 < g$–$r < 1.0$. (Figure 5 in B03). For the theoretical relations, Z09 is based on a library of stellar population models from the 2007 version of BC03 (CB07), which covers from 0 to 20 Gyr in age, six values in metallicity (Z = 0.0001 to 0.05), and spans a range of $-0.3 < g$-$i < 2.6$. IP13 is based on a sample of stellar population models from the Padova isochrones, which covers from 0.1 to 12.6 Gyr in age, seven values in metallicity (Z = 0.0001, 0.0004, 0.001, 0.004, 0.008, 0.019, and 0.03), and spans a range from $0.25 < g$–$r <$ 0.75. RC15 is also based on stellar population models from BC03 or FSPS, which spans a range of $-0.25 < g$–$r < 1.65$ for RC15(BC03) and a range of $-0.1 < g$–$r < 1.65$ for RC15(FSPS) (Figure 7 in RC15). By comparison, the sample of observed data of LSBGs (Section 2) has a range of $\mu_r > 21$ mag arcsec^{-2} and $r > 17.5$ mag, and 73% of the sample is bluer than g–$r = 0.4$. In Table 1, we tabulate these five representative CMLRs of B03, IP13, Z09, RC15(BC03), and RC15(FSPS) in the r, i, z, J, H, and K bands with g–r as the color indicator.

Figure 2 presents the stellar mass-to-light ratios (γ_*) in j band (γ_*^j, $j = g$, r, i, z, J, H, K) predicted by each CMLR (Table 1) for the sample, showing the beads-on-a-string nature of γ_* from the single color-based CMLR method. It shows that the CMLR-based method fails to reproduce the intrinsic scatter of γ_* expected from variations in star formation histories (SFH). In each panel, the γ_* from different CMLRs differ from each other due to distinct choices of initial mass function (IMF), star formation history (SFH), and stellar evolutionary tracks by different CMLR models.

Different IMFs primarily differ in the treatment of low-mass stars. The IMF that includes a larger number of low-mass stars normally produces a higher γ^* at a given color than the IMFs incorporating a smaller number of low-mass stars. This is in principle because the low-mass stars could greatly enhance the stellar mass but alter the luminosity little. Therefore, diverse IMFs would predominantly lead to a difference in the zero-point of CMLRs. For example, stellar mass estimates based on a Chabrier or Salpeter IMF differ by 0.3 dex, with the latter being higher (Roediger & Courteau 2015). As listed in Table 1, B03 adopts a "diet" Salpeter IMF, which includes more low-mass stars than the Chabrier IMF used by RC15 and Z09 CMLRs and the Kroupa (1998) IMF used by IP13 CMLR, so B03 gives a higher γ^* than other CMLRs at a given color (Figure 2).

Galaxies are expected to have a wide range of SFHs. The best-fit stellar mass could be significantly changed by different SFHs, in particular, depending on whether the SFH is continuous (rising/declining) or bursty. Any burst of star formation will bias the models toward lower γ_* values than the smooth star formation models at a given color. The uncertainties of γ_* in the optical that are due to different SFHs are ∼0.2 dex for quiescent galaxies, ∼0.3 dex for star-forming galaxies (Kauffmann et al. 2003), ∼0.5 dex at a given B-R, and could be up to 0.6 dex in extreme cases (Courteau et al. 2014). For the CMLRs in this work, IP13 adopts a single-component model of an exponential SFH, while the other CMLRs in this work are all based on two-component SFH models. Z09

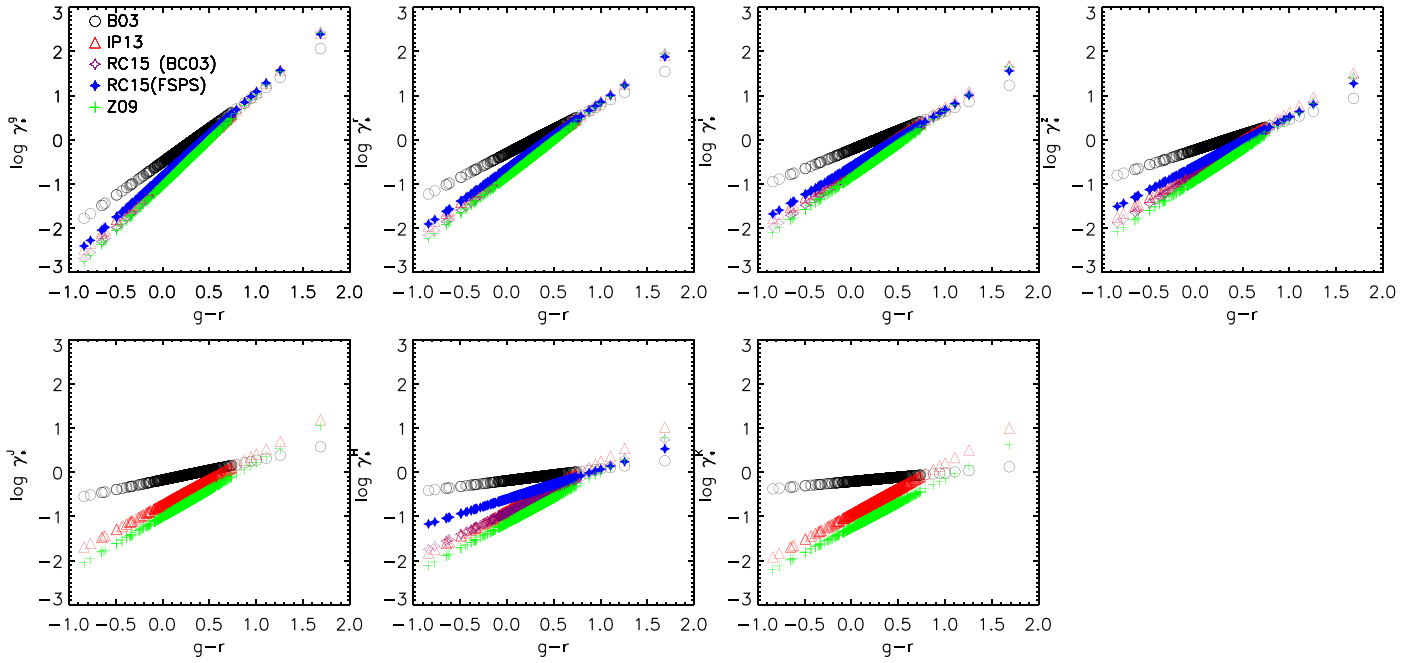

Figure 2. Relation between g–r color and log γ^{*j} ($j = g$, r, i, z, J, H, and K bands) from the CMLRs of B03 with an assumption of a "diet" Salpeter IMF (black circles), Z09 with an assumption of a Chabrier (2003) IMF (green plus), IP13 with an assumption of a Kroupa (1998) IMF (red triangles), RC15(BC03) with an assumption of a Chabrier (2003) IMF (open purple stars), and RC15(FSPS) with an assumption of a Chabrier (2003) IMF (filled blue stars).

Table 2
Mean (Upper) and Median (Lower) Stellar Mass Predicted by the Original (Left Part) and Recalibrated CMLRs (Right Part) for the LSBG Sample

Band	B03	IP13	R15(BC03)	R15(FSPS)	Z09	B03	IP13	R15(BC03)	R15(FSPS)	Z09
g	8.64	8.43	8.30	8.44	8.26	8.64	8.43	8.30	8.44	8.26
r	8.65	8.43	8.31	8.42	8.27	8.65	8.43	8.31	8.42	8.27
i	8.73	8.48	8.35	8.47	8.29	8.66	8.42	8.32	8.43	8.28
z	8.70	8.44	8.30	8.46	8.21	8.66	8.42	8.32	8.43	8.28
J	8.68	8.30	⋯	⋯	8.06	8.62	8.38	⋯	⋯	8.24
H	8.68	8.21	8.15	8.38	7.97	8.62	8.37	8.28	8.39	8.23
K	8.75	8.26	⋯	⋯	7.97	8.64	8.38	⋯	⋯	8.24
g	8.75	8.55	8.42	8.56	8.38	8.75	8.55	8.42	8.56	8.38
r	8.76	8.55	8.43	8.54	8.39	8.76	8.55	8.43	8.54	8.39
i	8.84	8.60	8.46	8.59	8.40	8.77	8.54	8.43	8.55	8.39
z	8.82	8.55	8.42	8.58	8.32	8.77	8.54	8.44	8.55	8.39
J	8.83	8.43	⋯	⋯	8.20	8.77	8.52	⋯	⋯	8.38
H	8.80	8.33	8.28	8.51	8.09	8.75	8.49	8.4	8.52	8.35
K	8.88	8.38	⋯	⋯	8.08	8.77	8.49	⋯	⋯	8.35

and RC15 (BC03) both consider the exponentially declining SFHs with a variety of random bursts superimposed. RC15 (FSPS) uses the exponential SFH with only one instantaneous burst added. B03 assumes the exponential SFH (starting from 12 Gyr in the past) with bursts superimposed, but limits the strength of bursts to $\leqslant$10% by mass, which constrains the burst events to only take place in the last 2 Gyr, so it is relatively smooth.

In Figure 2 the discrepancies in γ_* among the CMLRs in the NIR bands (J, H, and K) are obviously larger than the discrepancies in the optical bands (*griz*). This primarily rises from the different treatments of the TP-AGB stars, which are the low- to intermediate-mass stars ($0.6 \sim 10\,M_\odot$) in their late life stage, and emit a considerable amount of light in the NIR but little light in the optical. As listed in Table 1, B03 and RC15 (BC03) adopt a simplified prescription (Girardi et al. 2000, 2002) for TP-AGB stars, whereas IP13, RC15 (FSPS), and Z09 consider a relatively new prescription (Marigo & Girardi 2007; Marigo et al. 2008) for TP-AGB stars. The latter prescription incorporates a larger number of TP-AGB stars, and would hence greatly enhance the NIR luminosity but alter the optical luminosiittlety l. This inevitably results in lower NIR γ_* but changes the optical γ_* little.

4. Stellar Mass

The average γ_* in the u band suffers more from the perturbations of the young luminous blue stars, which formed recently and radiated a significant amount of light in the blue bands but contribute little to the galaxy mass. Additionally, the SDSS u-band data are of low quality, therefore we exclude the u-band γ_* from the following analysis.

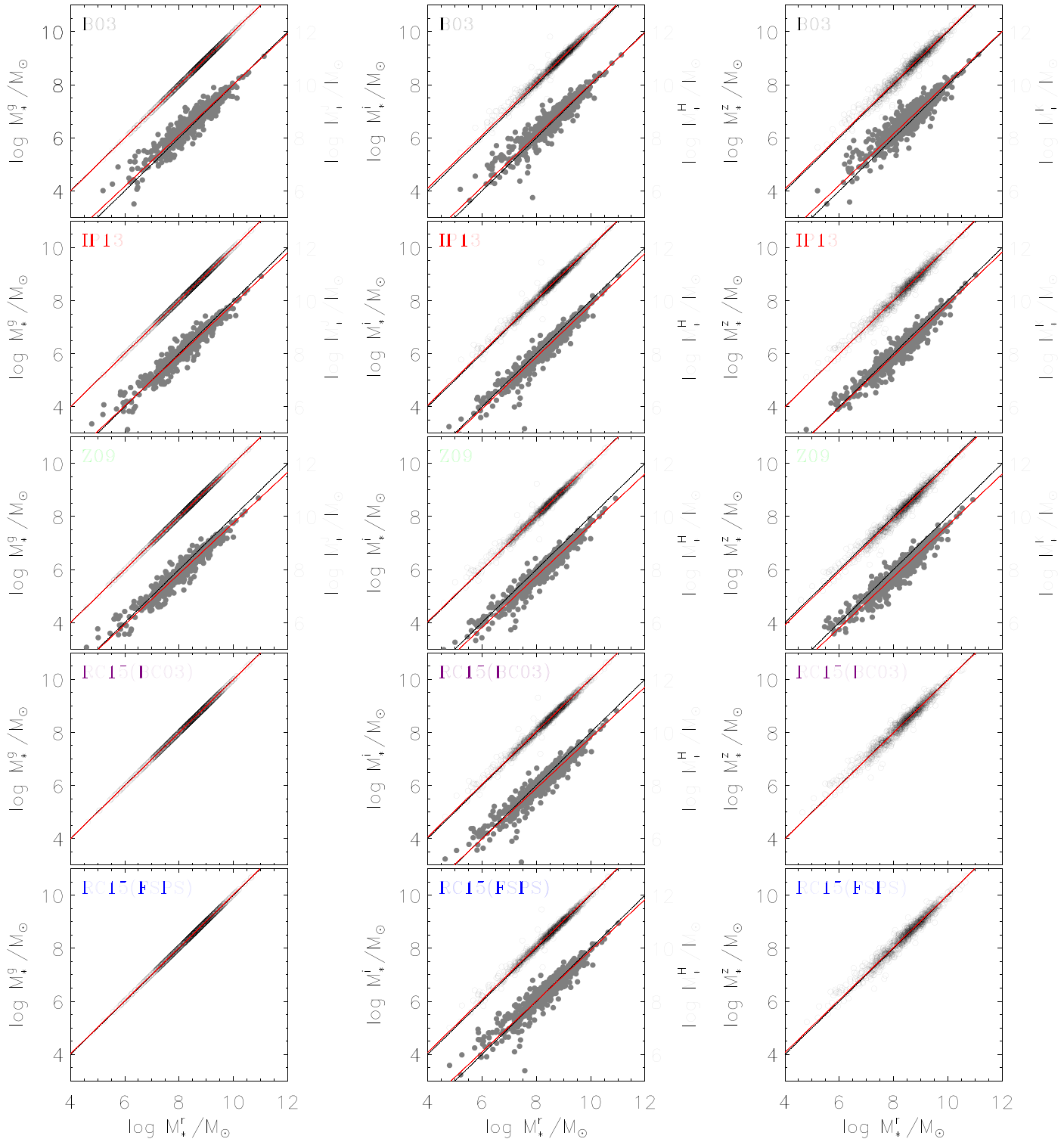

Figure 3. Stellar mass (M_*) estimates by different CMLRs of B03, IP13, Z09, RC15 (BC03), and RC15 (FSPS) listed in Table 1. For each CMLR, M_* estimates from g (open black circles) or J (filled gray circles) bands are plotted against M_* from r band (M_*^r) in the left panel. M_* estimates from i (open black circles) or H (filled gray circles) bands are plotted against M_*^r in the middle panel. M_* estimates from z (open black circles) or K (filled gray circles) bands are plotted against M_*^r in the right panel. For each panel, the two cases are offset for clarity, and the dashed black lines are the line of unity, and the red solid lines are the fit to the data. If the CMLR were internally self-consistent, the data would follow the line of unity (dashed black line). However, the fit line that the data follow obviously deviates from the line of unity, expect for data of g v.s. r bands. It should be noted that RC15 does not provide relations in J and K bands.

For the LSBG sample, we predict γ_*^j ($j = g, r, i, z, J, H$, and K bands) by each independent CMLR with g–r as the color indicator (Table 1), as g–r serves as a good color indicator for γ_*. The predicted γ_*^j are then multiplied by luminosities in the j band (Section 2.2) to produce M_* estimates from the j band (M_*^j). We list the mean and the median M_*^j originally by each CMLR for the sample in the left part in Table 2.

We can check the external consistency of different CMLRs by comparing M_* from different CMLRs. It is apparent that the five CMLRs produce distinct M_*^j estimates from the j band

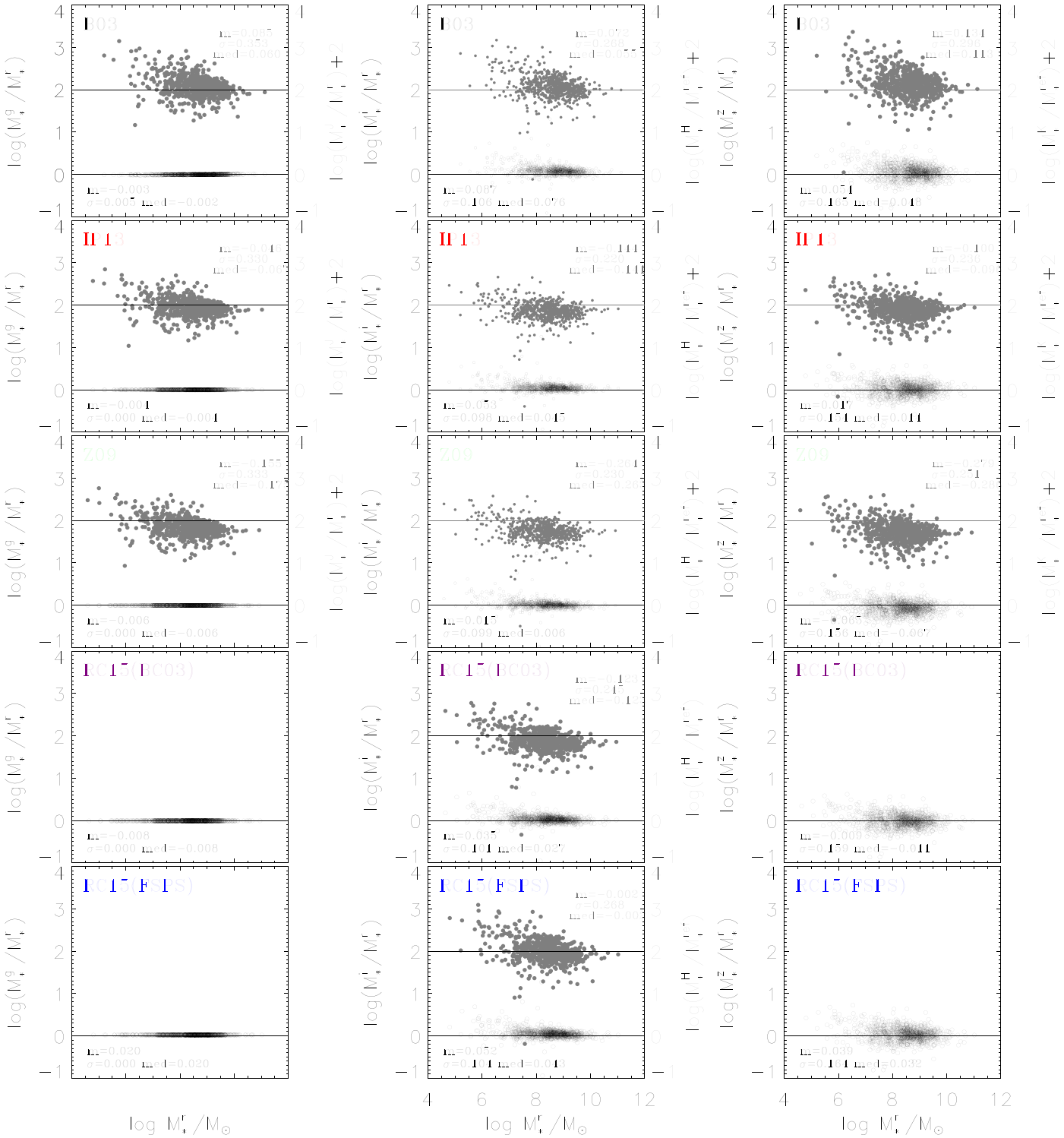

Figure 4. Residuals of data from the line of unity in each panel in Figure 3. For each CMLR, the residuals of the data from the line of unity in the g, i, and z bands are shown as open black circles in the lower region of the left, middle, and right panels, respectively. For clarity, residuals of the data from the line of unity in J, H, and K bands are offset by +2 and are shown as filled gray circles in the upper region of the left, middle, and right panels, respectively. The solid black and gray lines in each panel are the zero-residual lines for the corresponding data.

($j = g$, r, i, z, J, H, and K bands). In the same j band, B03 gives the highest M_*, while Z09 yields the lowest M_* for the sample. The difference between M_* predicted by B03 and Z09 is $0.3 \sim 0.5$ dex in the optical bands, and dramatically rises to $0.6 \sim 0.8$ dex in NIR bands due to the different treatments for TP-AGB stars (Section 3). The external inconsistency is caused by the different choices of the IMF, SFH, and SPS models.

We can examine each CMLR for the internal consistency from different bands. For any individual CMLR, M_* predicted from the g band (M_*^g) is closely consistent with M_* predicted from the r band (M_*^r). However, M_*^j ($j = i$, z, J, H, and K), especially $j = J$, H, and K, deviate from M_*^r to varying degrees, and the deviation is progressively increasing as the band becomes redder. For instance, the deviation of $M_*^{\rm NIR}$ from M_*^r

Table 3
Self-Consistent Stellar Masses

model	B_i	$\log M_0^i$	B_z	$\log M_0^z$	B_J	$\log M_0^J$	B_H	$\log M_0^H$	B_K	$\log M_0^K$
B03	0.994	20.609	0.994	16.132	0.965	10.288	0.988	13.395	0.981	14.738
IP13	0.995	17.362	1.005	6.132	0.969	6.302	0.995	−21.17	0.988	0.482
Z09	0.994	9.032	1.004	28.181	0.968	2.897	0.984	−7.583	0.983	−8.188
RC15(BC03)	0.992	11.488	0.999	−8.445	⋯	⋯	0.981	1.729	⋯	⋯
RC15(FSPS)	0.992	13.331	0.991	11.927	⋯	⋯	0.976	7.872	⋯	⋯

Note. The coefficients are for the solid red lines in Figure 3 in the function form of Equation (2).

is 0.1 dex by B03, −0.3 dex by Z09, and $-0.1 \sim -0.3$ dex by the three other CMLRs. This implies that B03 is nearly internally self-consistent in its M_* estimate from different bands, but it has a weak tendency to overestimate M_* estimates from NIR bands, whereas the four other CMLRs all underestimate M_* from NIR bands compared with M_*^r.

In Figure 3 we show M_*^j ($j = g$, r, i, z, J, H, and K) against M_*^r predicted by each CMLR for the sample (open black circles or filled gray circles). For each panel, the dashed black lines represent the line of unity for the data. If the CMLR were internally self-consistent in the M_* estimate from band to band, the data should exactly follow the line of unity. However, it does not seem to be the fact given that the data (open black circles or filled gray circles) in each panel obviously deviate from the line of unity (dashed black lines) to different degrees, except for the data in the panel of M_*^g versus M_*^r. This demonstrates that M_*^g is highly consistent with M_*^r, while M_*^j ($j = i$, z, J, H, and K) deviates from M_*^r, and the deviation progressively increases as the band becomes redder. In order to clearly display the deviation of data from the line of unity, we plot the residuals of data from the line of unity in Figure 4. In the case of internal inconsistency of each CMLR from band to band, we calibrate each CMLR to be internally self-consistent in M_* estimates from different bands, based on the LSBG sample in Section 5.

5. Self-consistent *M/L*–Color Relations

5.1. Self-consistent Stellar Masses

For each individual CMLR, the M_* estimates from g band (M_*^g) closely agree with those from r band (M_*^r) for the sample. However, the M_* estimates from the i, z, J, H, and K bands differ from M_*^r for the sample to varying degrees (Section 4). Assuming M_*^r as the reference M_* for a galaxy, we can fit the relations between M_*^j ($j = i$, z, J, H, and K) and M_*^r of the sample in the function form below, following MS14,

$$\log(M_*^j/M_0) = B_j \log(M_*^r/M_0), \quad (2)$$

where B_j is the slope of the linear fit line, and M_0 is the M_* where j band intersects r band. A "robust" bi-square weighted line-fit method is adopted to fit data of the LSBG sample. The fit lines are overplotted as solid red lines in each panel in Figure 3, which deviate from the line of unity in the panels of the i, z, J, H, and K bands, demonstrating the problem of self-inconsistency in M_* estimates from different bands for the same sample. The coefficients from the fit are tabulated in Table 3.

5.2. Recalibrated CMLRs

According to the coefficients in Table 3, we renormalize M_*^j ($j = i$, z, J, H, and K) to the reference mass M_*^r. Then, the renormalized M_*^j ($M_{*,\mathrm{re}}^j$) were divided by the luminosity in j band to generate the renormalized γ_*^j ($\gamma_{*,\mathrm{re}}^j$). Next, the $\gamma_{*,\mathrm{re}}^j$ were plotted against g–r in Figure 5. For each panel, galaxies of the LSBG sample are shown as open black circles, which show clear correlations between $\gamma_{*,\mathrm{re}}^j$ and g–r color. We then fit the relations between the $\gamma_{*,\mathrm{re}}^j$ and g–r in the function form of Equation (1) using the biweight line-fit method. The fit line is overplotted as the solid red line in each panel in Figure 5, and the solid blue line represents the original CMLRs (Table 1) for comparison. The recalibrated CMLRs are tabulated in Table 4, which could produce internally self-consistent M_* estimates from different bands for the galaxy, and this self-consistent M_* should be highly consistent with the assumed reference mass, which is M_*^r in this work.

Compared with M_*^r, the original B03 slightly overestimated M_* from NIR bands (M_*^{NIR}) while the four other original CMLRs underestimated M_*^{NIR} (Table 2). After recalibration, the overestimate or underestimate are corrected correspondingly. As shown in each panel in Figure 5, the recalibrated B03 is below the original relation (solid blue line), and the four other recalibrated relations of Z09, IP13, RC15 (BC03), and RC15 (FSPS) are all above the original relation, especially in the NIR bands. Furthermore, the original relation of B03 requires the smallest corrections, while the original Z09 relations require the largest corrections in each band, in particular in the NIR bands. This is because Z09 is based on the prescription for the TP-AGB phase, which incorporates a larger number of TP-AGB stars. It can greatly enhance the luminosities in the NIR but alters the luminosities in the optical little, which inevitably results in a lower γ_* from the NIR bands than from the optical bands.

6. Discussion

6.1. Secondary Color Dependence

g–r acts as a primary color indicator of γ_* (Figure 5). In this section, we examine whether the recalibrated CMLRs based on g–r could be improved further by including r-z or J–K as a secondary color term. First, we plot $\gamma_{*,\mathrm{re}}^j$ against r–z (Figure 6) or J–K (Figure 7) for each CMLR. Although it appears that $\gamma_{*,\mathrm{re}}^j$ depends little on either r–z or J–K, the two colors could not be completely avoided without a further examination in quantity. For convenience, we denote γ_* from the j band predicted by the recalibrated CMLRs (Table 4) $\gamma_{*,\mathrm{rec}}^j$, and those predicted by the renormalized M_*^j (Table 3) $\gamma_{*,\mathrm{re}}^j$ ($j = i$, z, J, H, K). The residuals of $\gamma_{*,\mathrm{rec}}^j$ from $\gamma_{*,\mathrm{re}}^j$ are denoted Δ^j ($\Delta^j = \gamma_{*,\mathrm{re}}^j - \gamma_{*,\mathrm{rec}}^j$),

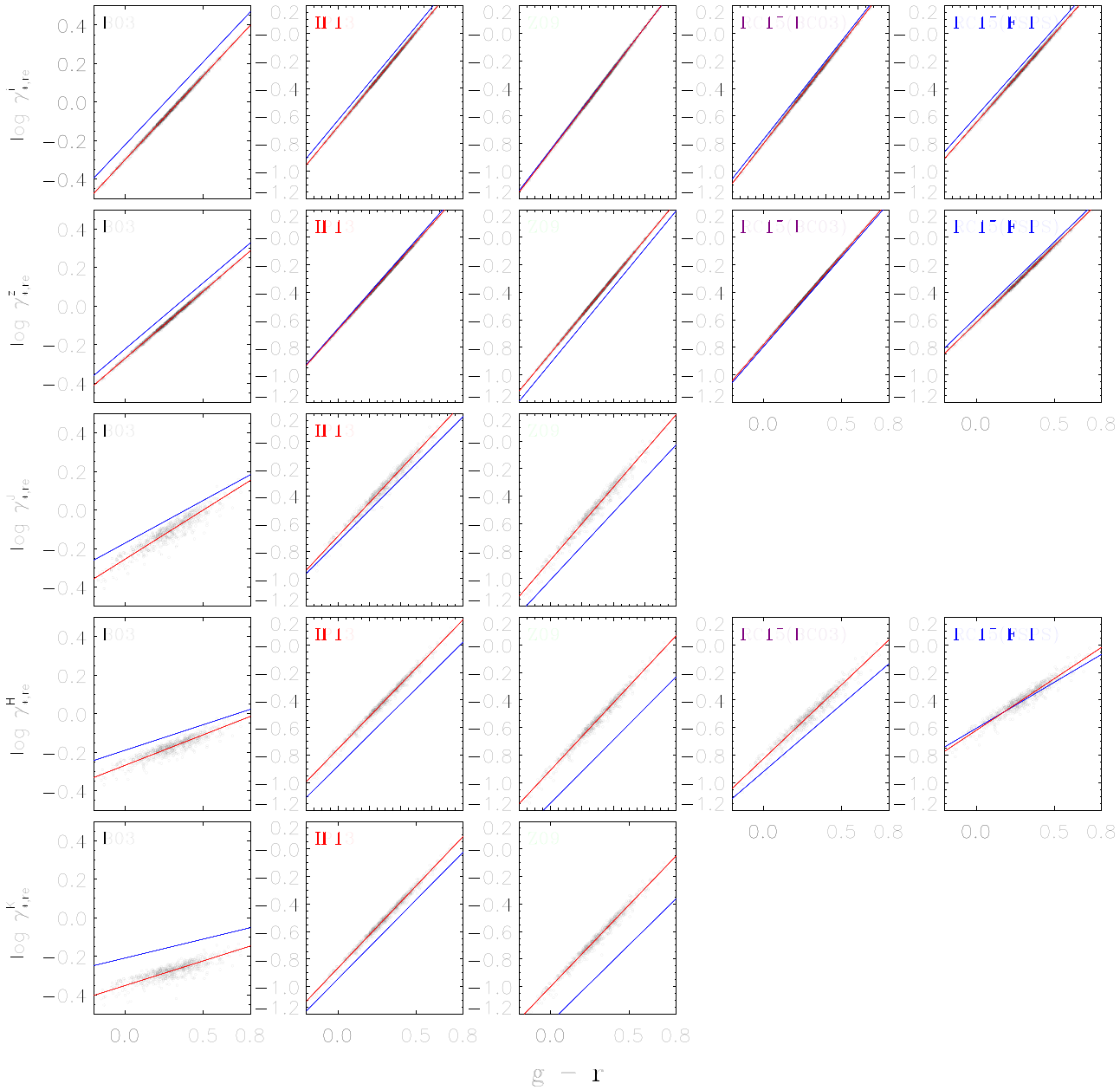

Figure 5. Renormalized stellar mass-to-light ratios ($\gamma^j_{*,\mathrm{re}}$, $j = i, z, J, H$, and K) in logarithm as a function of g–r color. Galaxies in the sample are shown as open black circles in each panel, where the solid red line represents the fit relation between log $\gamma^j_{*,\mathrm{re}}$ and g–r, and the blue line represents the original relation for comparison.

which are in fact the difference between the data (open black circles) and the recalibrated line (solid red line) in each panel in Figure 5.

If Δ^j is dependent on the colors of r-z or r-z, the recalibrated CMLR based on g–r color alone could be improved by Equation (3),

$$\log \gamma^j_* = a_j + b_j \times (\mathrm{g} - \mathrm{r}) + \Delta^j. \quad (3)$$

In order to check whether Δ^j depends on r-z or J–K , we additionally plot Δ^j against r–z (Figure 8) or J–K (Figure 9), and fit a linear relation between Δ^j and the color in each panel (solid red line). It shows that the fit line is almost flat and completely overlaps the zero-residual line (black line), implying that Δ^j depends little on the color of either r–z or J–K. Therefore, there is no need for a secondary color term based on r–z or J–K (Δ^j in Equation (3)) to improve the recalibrated CMLRs in this work. This demonstrates that the variation of γ_* can be well traced by the optical color but is minimized in NIR color, which has already been proved in McGaugh & Schombert (2014), who changed the age of the solar metallicity stellar population of Schombert & Rakos (2009) from 1 to 12 Gyr, and the induced changes in B–V are 0.37 mag but only 0.03 mag in J–K.

6.2. Error Budget

The typical γ_* uncertainties are ∼0.1 (∼0.2) dex in the optical (NIR) for B03, ∼0.1 dex for IP13, and 0.1 ∼ 0.15 dex for Z09. For RC15, it could be deduced (from their Figures 2

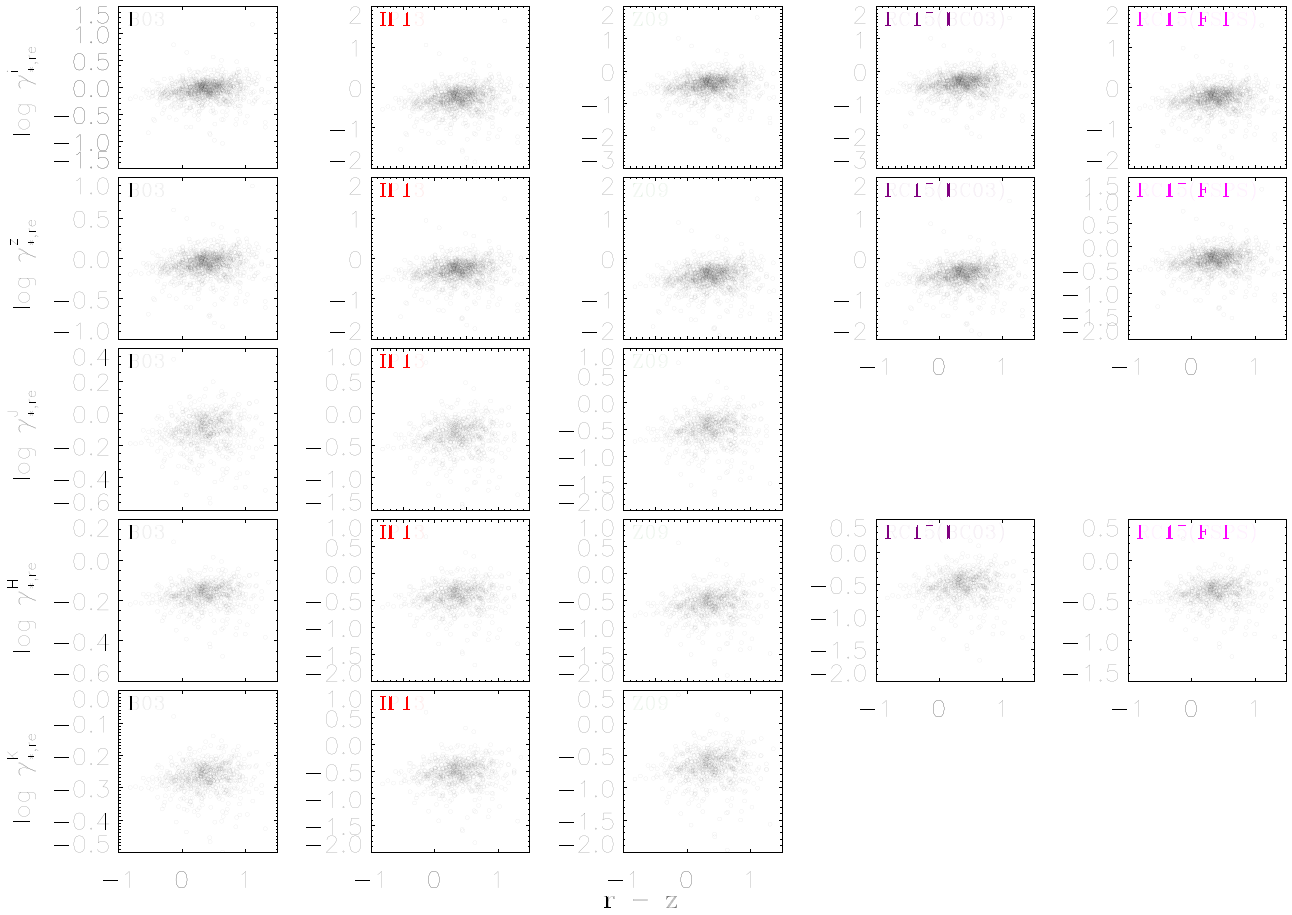

Figure 6. Renormalized stellar mass-to-light ratios ($\gamma^j_{*,\mathrm{re}}$, $j = i$, z, J, H, and K) in logrithm as a function of r–z color. The illustrations are similar to Figure 5.

Table 4
Recalibrated CMLRs

Model	a_r	b_r	a_i	b_i	a_z	b_z	a_J	b_J	a_H	b_H	a_K	b_K
B03	−0.306	1.097	−0.299	0.874	−0.272	0.699	−0.245	0.499	−0.253	0.283	−0.333	0.226
IP13	−0.663	1.530	−0.679	1.380	−0.674	1.280	−0.684	1.199	−0.742	1.138	−0.860	1.175
Z09	−0.840	1.654	−0.854	1.495	−0.842	1.374	−0.852	1.291	−0.896	1.178	−0.990	1.150
RC15(BC03)	−0.792	1.629	−0.801	1.456	−0.781	1.308	⋯	⋯	−0.803	1.017	⋯	⋯
RC15(FSPS)	−0.647	1.497	−0.648	1.298	−0.619	1.120	⋯	⋯	−0.604	0.714	⋯	⋯

Note. The coefficients are for the solid red lines in Figure 5 in the function form of Equation (1).

and 3 in RC15) that the scatter in γ_* from the BC03 model is ∼0.1 dex, but the scatter from the FSPS model is not clearly available. These typical uncertainties, which are inherent in the original CMLRs, should be directly transplanted into the recalibrated CMLRs in this work, because the recalibrating in this work does not change the models on which the CMLRs are based. For the LSBG sample, the uncertainty in γ_* predicted by a CMLR should be a combination of the inherent uncertainty in the CMLR and the photometric error. The uncertainty in g–r color of the LSBG sample in this work is <0.08 mag for 95% of the galaxies, which would be ultimately propagated to be uncertainties of ∼0.08 (∼0.03), ∼0.11 (∼0.10), ∼0.11 (∼0.10), ∼0.11 (∼0.08), and ∼0.10 (∼0.05) dex in log γ_* predicted in optical (NIR) bands by the recalibrated relations, and almost the same values of uncertainties in log γ_* predicted by original relations of B03, IP13, Z09, RC15 (BC03), and RC15 (FSPS), respectively. For this LSBG sample, the total uncertainties in γ_* predicted by each CMLR before or after recalibration are therefore almost the same.

6.3. γ_* and M_* from Recalibrated CMLRs

In Table 4, γ_* from the j band was estimated by each independent recalibrated CMLR at g–$r = 0.3$ ($\gamma^j_{0.3}$, $j = i$ z, J, H, K), which is the mean of the color distribution of the sample in this work, and γ^j_* at g–$r = 0.6$ ($\gamma^j_{0.6}$) was also tabulated in order to give an indication for γ^j_* estimates at some redder color by these recalibrated CMLRs. In addition, the originally predicted γ^j_* was also listed for comparison.

Apparently, B03 always gives the highest γ^j_*, and Z09 gives the lowest values, regardless of whether this value is taken before or after recalibration, which is primarily due to the differences in the IMF. In quantity, the span in the originally predicted γ^j_* is ∼0.44, ∼0.48, ∼0.60 ∼0.69, and ∼0.77 dex at

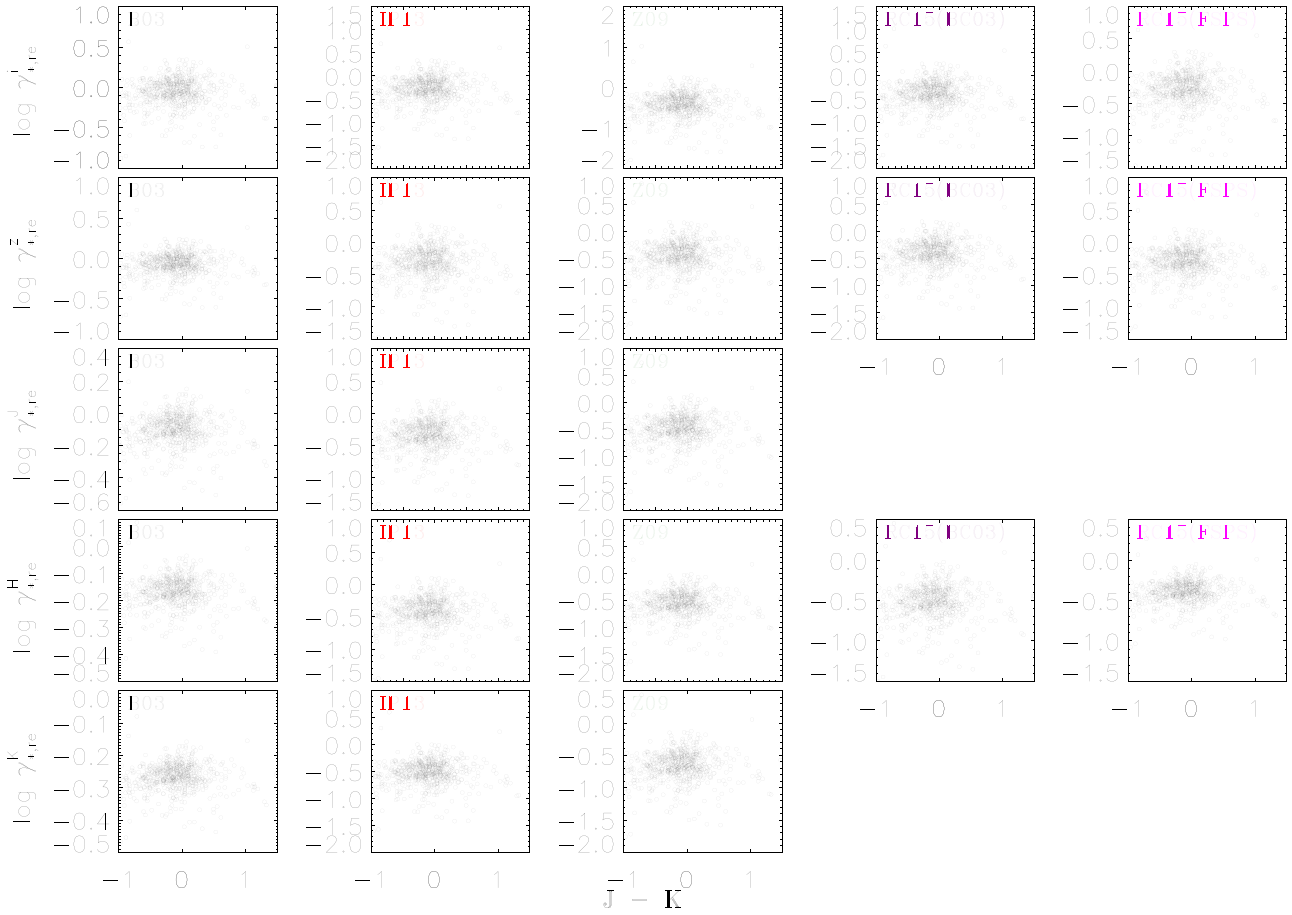

Figure 7. Renormalized stellar mass-to-light ratios ($\gamma^{j}_{*,\mathrm{re}}$, $j = i$, z, J, H, and K) in logrithm as a function of J–K color. The illustrations are similar to Figure 5.

the blue color (g–$r = 0.3$), and ∼0.25, ∼0.28 ∼0.37, ∼0.42, and ∼0.49 dex at the redder color (g–$r = 0.6$) for $j = i$, z, J, H, and K bands, respectively. In contrast, the span in γ^{j}_{*} predicted by the recalibrated relations has been greatly narrowed to ∼0.37, ∼0.37, ∼0.37, ∼0.36, and ∼0.36 dex at the blue color, and to ∼0.18, ∼0.16, ∼0.12, ∼0.09, and ∼0.09 dex at the red color in the corresponding bands. This clearly shows that the range in γ^{j}_{*} by recalibrated CMLRs is much narrower than originally predicted, especially in the NIR bands. This demonstrates that the NIR luminosities are more robust than the optical luminosities in predicting the γ_{*} of galaxies. It is worth noting that the uncertainties (Section 6.2) in γ_{*} predicted by the original or recalibrated relation for each CMLR are almost the same, so these errors do not alter the comparison above.

We can examine each recalibrated CMLR for the internal consistency in M_{*} from band to band. We list the mean and median M_{*} predicted by each recalibrated CMLR in the right part in Table 2. It is apparent that M^{j}_{*} ($j = g$, i, z, J, H, and K) is highly consistent with M^{r}_{*}, which is the reference stellar mass. For instance, the difference of M^{j}_{*} from M^{r}_{*} is reduced to 0.03 dex (from the original 0.1 dex) by B03, 0.04 dex (from the original 0.3 dex) by Z09, 0.06 dex (from the original 0.27 dex) by IP13, and 0.03 dex (from the original 0.1–0.2 dex) by RC15 CMLRs after recalibration. This demonstrates that each CMLR could produce internally self-consistent M_{*} after recalibration when it is applied in different photometric bands.

6.4. Comparison with MS14

In the pioneering work of MS14, several CMLRs were recalibrated in filters of *V, I, K*, or [3.6] based on a sample of disk galaxies (B–V as the color indicator). In this work, three CMLRs that are in common with MS14 were recalibrated, but in SDSS and NIR filters of r, i, z, J, H, or K based on a sample of LSBGs (g–r as the color indicator). We therefore compare our recalibrated relations with those of MS14 for the three CMLRs that are in common (B03, IP13, and Z09) in the common K band in this section.

In MS14, the γ_{*} from K band at B–$V = 0.6$ ($\gamma^{\mathrm{K}}_{B-V=0.6}$) predicted by their recalibrated relations is 0.60, 0.54 and 0.50 $M_{\odot}/L_{\odot}$ by B03, IP13, and Z09, respectively. In contrast, the originally predicted $\gamma^{\mathrm{K}}_{B-V=0.6}$ are correspondingly 0.73, 0.41, and 0.21 $M_{\odot}/L_{\odot}$ (the last column in Table 5). It is apparent that the range in $\gamma^{\mathrm{K}}_{B-V=0.6}$ has been enormously narrowed to 0.08 dex from the original 0.54 dex by their recalibrations. In order to compare with MS14, we additionally tabulate γ^{K} at g–$r = 0.4$ ($\gamma^{\mathrm{K}}_{0.4}$) predicted by our recalibrated relations, which is ∼0.57, ∼0.41, and ∼0.30 $M_{\odot}/L_{\odot}$ by B03, IP13, and Z09 (Table 5) because g–$r = 0.4$ is equivalent to B–$V = 0.6$ according to the filter transformation prescriptions of Smith et al. (2002). By comparison, the originally predicted $\gamma^{\mathrm{K}}_{0.4}$ is 0.74, 0.33, and 0.16 $M_{\odot}/L_{\odot}$, so the range in $\gamma^{\mathrm{K}}_{0.4}$ has been reduced to ∼0.28 dex from the original ∼0.67 dex by our recalibrations. However, compared with $\gamma^{\mathrm{K}}_{B-V=0.6}$ predicted by MS14 recalibrated relations,

Figure 8. Δ^j ($j = i,z, J, H, K$) as a function of $r - z$. The black line is the zero-residual line, and the red line is the fit to the data, which nearly overlap the zero-residual line.

Table 5
Stellar Mass-to-light Ratios (γ_*) Predicted by Original and Recalibrated CMLRs

Model	$\gamma^i_{0.3}$	$\gamma^z_{0.3}$	$\gamma^J_{0.3}$	$\gamma^H_{0.3}$	$\gamma^K_{0.3}$	$\gamma^i_{0.6}$	$\gamma^z_{0.6}$	$\gamma^J_{0.6}$	$\gamma^H_{0.6}$	$\gamma^K_{0.6}$	$\gamma^K_{0.4}$	$\gamma^K_{B--V=0.6}$
Original CMLR models												
B03	1.09	0.96	0.91	0.78	0.71	1.98	1.55	1.24	0.93	0.81	0.74	0.73
IP13	0.60	0.53	0.41	0.29	0.25	1.55	1.29	0.89	0.63	0.56	0.33	0.41
Z09	0.40	0.32	0.23	0.16	0.12	1.11	0.82	0.53	0.35	0.26	0.16	0.21
RC15B	0.46	0.39	⋯	0.24	⋯	1.24	0.97	⋯	0.47	⋯	⋯	⋯
RC15F	0.61	0.56	⋯	0.40	⋯	1.47	1.20	⋯	0.63	⋯	⋯	⋯
Recalibrated CMLR models												
B03	0.92	0.87	0.79	0.67	0.53	1.68	1.40	1.13	0.84	0.63	0.56	0.60
IP13	0.54	0.51	0.47	0.40	0.31	1.41	1.24	1.09	0.89	0.71	0.41	0.54
Z09	0.39	0.37	0.34	0.29	0.23	1.11	0.96	0.85	0.67	0.51	0.30	0.50
RC15(BC03)	0.43	0.41	⋯	0.31	⋯	1.18	1.01	⋯	0.66	⋯	⋯	⋯
RC15(FSPS)	0.55	0.52	⋯	0.40	⋯	1.35	1.13	⋯	0.68	⋯	⋯	⋯

Note. The stellar mass-to-light ratios predicted from different bands (i, z, J, H, K) by each CMLR before (Table 1) and after recalibration (Table 4) are given at g–$r = 0.3$ (the mean and median colors of the LSBG sample) and g–$r = 0.6$. Additionally, γ_* predicted by MS14 from K band at B–$V = 0.6$ ($\gamma^K_{B-V=0.6}$) is listed, and for comparison, γ_* predicted by our recalibrated relations (Table 4) in Section 5 from K band at g–$r = 0.4$ ($\gamma^K_{0.4}$) is also given for comparison because g–$r = 0.4$ is equivalent to B–$V = 0.6$ according to the filter transformation prescription of Smith et al. (2002).

$\gamma^K_{0.4}$ predicted by our recalibrated relations in this work is 0.03, 0.09, 0.26 dex lower than that of B03, IP13, and Z09, respectively.

In order to determine the sources of the differences, we examined the three different ingredients between this work and MS14, which are the independent procedures, the different assumptions of reference M_*, and the distinct data sets.

For the procedures, although the procedure in this work was coded to implement the same methodology as adopted by MS14, it is independent of and not identical with the MS14 procedure. We therefore investigate the possible offset in recalibrated relations that is due to the minor differences between the procedures of MS14 and our

Figure 9. Δ^{j} ($j = i,z,J,H,K$) as a function of J–K. The black line is the zero-residual line, and the red line is the fit to the data, which nearly overlap the zero-residual line.

procedures, by repeating the exact work of MS14 on their data using our procedures. It was found that compared with the MS14 procedures, our procedures would drag $\gamma^{K}_{B-V=0.6}$ down by 0.05, 0.01, and 0.04 dex for B03, IP13, and Z09, respectively. These minor offsets in $\gamma^{K}_{B-V=0.6}$ caused by the minor differences between our and the MS14 procedures are denoted Δ^{K}_{pro} for convenience (Table A1).

For the assumption of reference M_*, we assumed M_* estimates from the SDSS r band (M^r_*) as the reference M_* to which M_* estimates from other filter bands were renormalized in this work, while MS14 assumed M_* from the Johnson V band (M^V_*) as their reference M_*. The different assumptions are the choices in the different filter systems (SDSS versus Johnson–Cousins), but it is necessary to investigate the possible offset in recalibrated relations due to the different choices of reference M_* between this work and MS14 (M^r_*-based versus M^V_*-based). We present the investigation in the Appendix, where we conclude that $\gamma^{K}_{B-V=0.6}$ predicted by the M^r_*-based recalibrated relations is 0.03, 0.11, and 0.23 dex lower than those predicted by M^V_*-based recalibrated relations. These major offsets in $\gamma^{K}_{B-V=0.6}$ caused by the different assumptions of the reference M_* are denoted Δ^{K}_{ref} for convenience (Table A1).

In this case, for the three CMLRs in common of B03, IP13, and Z09, the apparent differences (0.03, 0.09, and 0.26 dex) between $\gamma^{K}_{0.4}$ (this work) and $\gamma^{K}_{B-V=0.6}$ (MS14) could be completely explained by the combination of Δ^{K}_{ref} (0.03, 0.11, and 0.23 dex) and Δ^{K}_{pro} (0.05, 0.01, and 0.04 dex; Table A1). This implies that the apparent differences between our recalibrated relations in this work and those in MS14 in the common K band are totally caused by the systematic offsets due to the major differences in the assumptions of reference mass and the minor differences in procedures between this work and MS14. Therefore, taking into account the different assumptions of reference mass and the independent procedures, our recalibrated CMLRs based on a sample of LSBGs in this work yield very consistent γ_* in the common K band with the recalibrated CMLRs based on a sample of disk galaxies by MS14 . So there is no room left for any apparent difference in the recalibrated relations introduced by the possible difference of our LSBG sample from the disk galaxy sample in MS14.

It is beyond the scope of this work and also difficult to evaluate which assumption of reference mass is better because the different assumptions are only the choices in different filter systems (SDSS versus Johnson–Cousins). Additionally, this work is motivated by recalibrating each individual CMLR to give internally self-consistent M_* for a same galaxy, when it is applied in different bands of SDSS and NIR filters, and the internally self-consistent M_* from any band predicted by each recalibrated CMLR should be highly consistent with the reference M_*. We therefore examine the offset between different reference M_* in the Appendix, which gives that M^r_* is systematically 0.11, 0.25, and 0.33 dex lower than M^V_* by B03, IP13, and Z09 (Table 6) for the same sample as in this work.

Table 6
Distribution (Mean, σ) of M_* from the SDSS r or Johnson V Bands of the LSBG Sample

Model	Mean(M_*^r)	$\sigma(M_*^r)$	Mean(M_*^V)	$\sigma(M_*^V)$	$\Delta_{\rm mean}$
B03	8.65	0.81	8.76	0.75	0.11
IP13	8.41	0.85	8.66	0.77	0.25
Z09	8.27	0.87	8.60	0.79	0.33

Note. The values are all logarithmic. M_*^r is estimated from the r-band luminosities with the g–r as the indicator color of γ_*^r. M_*^V is estimated from the V-band luminosities with B–V as the indicator color of γ_*^V. $\Delta_{\rm mean}$ is the difference of the mean value of the M_*^r distribution from that of the M_*^V distribution.

7. Summary and Conclusions

Based on a sample of LSBGs, we examined five representative CMLRs of B03, IP13, Z09, RC15 (BC03), and RC15 (FSPS). For each individual CMLR, it gives different stellar mass (M_*) estimates for the same sample, when it is applied in different photometric bands of SDSS optical g, r, i, z, NIR J, H, and K. M_*^g closely agrees with M_*^r, but M_*^j ($j = i, z, J, H, K$) deviates from M_*^r, and the deviation is comparatively larger in the NIR bands. Assuming M_*^r as a reference M_*, we renormalized the M_* estimates from each of the other bands of j (M_*^j) to the reference mass, and subsequently obtained the recalibrated CMLR by fitting the relations between g–r and γ_*^j calculated from the renormalized M_*^j for each original CMLR ($j = i, z, J, H, K$). The g-r is the primary color indicator in the recalibrated relations, which depends little on r–z or J–K. Each recalibrated CMLR could produce internally self-consistent M_* estimates for the same galaxy, when it is applied in different bands of j ($j = r, i, z, J, H, K$), and the self-consistent M_* should be "the same as" or highly consistent with the reference mass of M_*^r. In addition, the differences in the original predicted γ_*^j by the five different CMLRs are largely reduced, particularly in the NIR bands.

Compared with the pioneering work of MS14, the γ_*^K predicted by the recalibrated CMLRs in this work is 0.03, 0.09, 0.26 dex lower than $\gamma_{B-V=0.6}^K$ predicted by MS14 recalibrations by B03, IP13, and Z09, respectively. These offsets could be fully explained by the combination of the major systematic offsets caused by the different choices of reference mass (0.03, 0.11, and 0.23 dex) and the minor systematic offsets caused by independent procedures (0.05, 0.01, and 0.04 dex) between this work and MS14. This implies that considering the major effect of different choices of reference M_* and the minor effect of independent procedures, the recalibrated CMLRs in this work based on a sample of LSBGs give very consistent γ_*^K with the recalibrated CMLRs by MS14 at the equivalent color. So there is no room left for any difference in the recalibrations caused by the possible bias of the LSB galaxy sample from the disk galaxy sample in MS14.

It is difficult to judge which choice of reference mass is better because the choices have to be made in different photometric filter systems. However, it is necessary to give the offsets between the final self-consistent M_* predicted by the recalibrated relations with different assumptions of the reference mass (M_*^r versus M_*^V). The M_*^r-based recalibrated relations in this work (Table 5) produce the final self-consistent M_*, which are systematically 0.11, 0.25, and 0.33 dex lower than those produced by the M_*^V-based recalibrated CMLRs in MS14, by B03, IP13, and Z09.

The authors appreciate the anonymous referee for their thorough reading and constructive comments. D.W. would like to gratefully acknowledge the China Scholarship Council (CSC) for the scholarship that enables her to be a visiting scholar to Professor S. Stacy McGaugh in the Astronomy Department at Case Western Reserve University (CWRU). The work presented in this paper was fully developed and completed during her visit at CWRU. D.W. is also supported by the National Natural Science Foundation of China (NSFC) grant Nos. U1931109, 11733006, the Young Researcher Grant funded by National Astronomical Observatories, Chinese Academy of Sciences (CAS), and the Youth Innovation Promotion Association, CAS.

Appendix
Effect of Reference Stellar Mass

The sample in this work has photometric data in the SDSS optical (u, g, r, i, z) and NIR J, H, K bands. In order to examine the possible effect of different assumptions of reference M_* (M_*^r versus M_*^V) on the recalibrated relations, we first transformed the magnitudes in SDSS g and r filters to Johnson B and V filters by using the transformation prescriptions of Smith et al. (2002) for the sample. This sample now has photometric data in both the SDSS filter and the Johnson–Cousins B and V bands and in the NIR J, H, and K bands.

For the sample, M_* from the V band (M_*^V) or r band (M_*^r) were predicted by the original CMLRs of B03, IP13 and Z09 (based on B–V color). When the distribution of M_*^V is compared with that of M_*^r, M_*^r is systematically 0.11, 0.25, and 0.33 dex lower than M_*^V by B03, IP13, and Z09 for this same sample ($\Delta_{\rm mean}$ in Table 6). This proves that the assumption of M_*^r as reference M_* would bias the baseline of M_* and the renormalized γ_* in each band toward lower values compared with the assumption of M_*^V as reference M_*.

In analogy to Section 5, we furthermore recalibrated each of the three CMLRs (B03, IP13, Z09) in K band (on B–V color) based on the sample of LSBGs, assuming M_*^V or M_*^r as reference M_*, respectively. More specifically, for each of the three CMLRs (B03, IP13, Z09), we first renormalized the M_* estimates from K band (M_*^K) to the reference mass of M_*^r, then divided the renormalized M_*^K by the K-band luminosity to obtain the renormalized γ_*^K ($\gamma_{*,\rm re}^K$), and ultimately fit the relations between $\gamma_{*,\rm re}^K$ and B–V color to obtain the recalibrated relations in K band, which is denoted as M_*^r-based recalibrated relations for convenience. Similarly, we obtained M_*^V-based recalibrated relations in m band by assuming the reference mass of M_*^V. These two sets of recalibrated CMLRs in K band are shown in Figures A1–A2, which clearly shows that compared with the M_*^V-based recalibrations (solid red line in Figures A2), the M_*^r-based recalibrated relations (solid red line in Figures A1) obviously dragged down $\gamma_{*,\rm re}$ in each panel for each CMLR, in particular, for IP13 and Z09, because the two figures share the same y-axis range and scale for convenient comparison.

In Table A1 we list γ_* in K band at B–$V = 0.6$ predicted by M_*^V-based ($\gamma_{B-V=0.6}^K(M_*^V)$) and M_*^r-based ($\gamma_{B-V=0.6}^K(M_*^r)$) recalibrated CMLRs, and $\gamma_{B-V=0.6}^K$ predicted by MS14 ($\gamma_{B-V=0.6}^K$(MS14)) for comparison. It is apparent that $\gamma_{B-V=0.6}^K(M_*^V)$ are very consistent with $\gamma_{B-V=0.6}^K$(MS14), which also assumed M_*^V as reference M_*, and the small differences between the two are caused by the minor

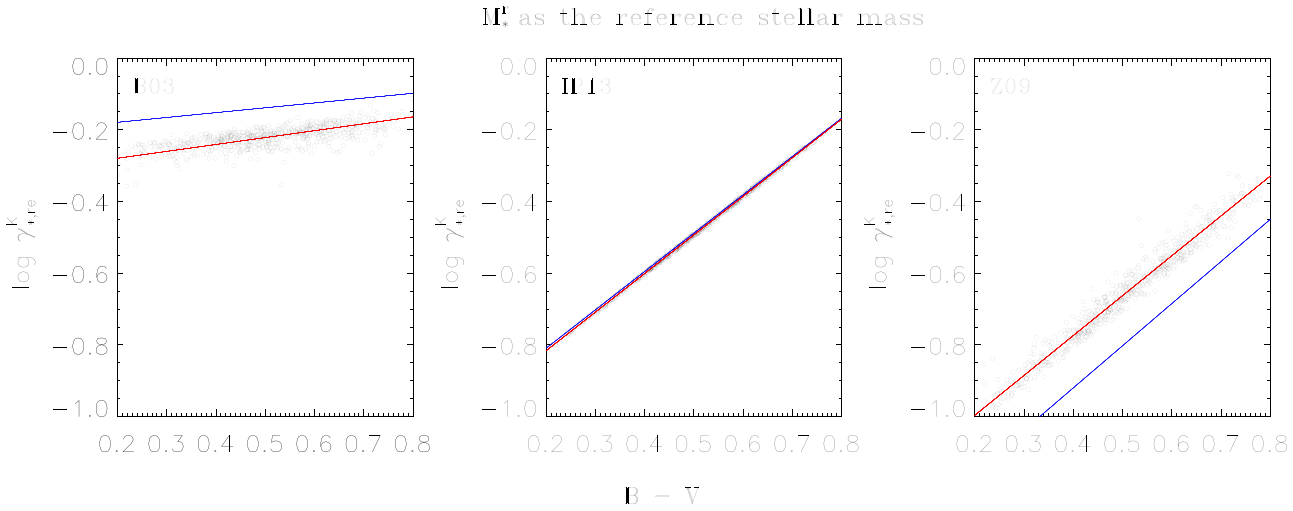

Figure A1. $\gamma^{K}_{*,re}$ from the stellar mass renormalized to M^r_* plotted against B–V color. For each panel, the black circles are galaxies of the LSBG sample, and the solid red line is the fit to the data (recalibrated CMLR), and the blue line is the original CMLR.

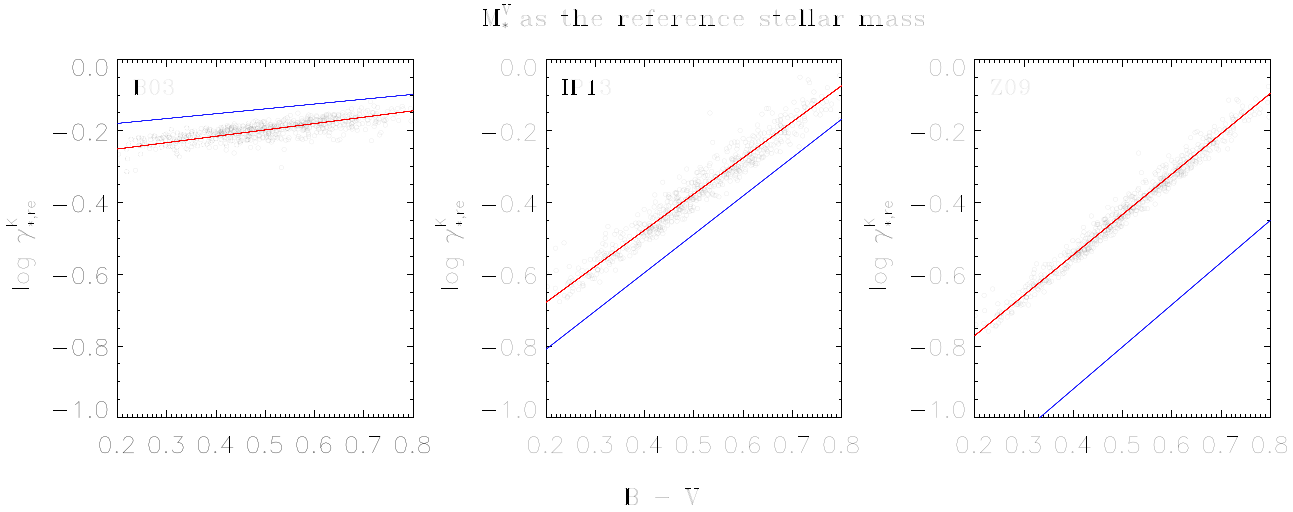

Figure A2. $\gamma^{K}_{*,re}$ from the stellar mass renormalized to M^V_* plotted against B–V color. For each panel, the black circles are galaxies of the LSBG sample, and the solid red line is the fit to the data (recalibrated CMLR), and the blue line is the original CMLR.

Table A1
γ^{K}_{*} Predicted by M^r_*-based or M^V_*-based Recalibrated CMLRs at B–$V = 0.6$ in This Work, and Those from M^V_*-based Recalibrations in MS14

Model	$\gamma^{K}_{B--V=0.6}(M^r_*)$	$\gamma^{K}_{B--V=0.6}(M^V_*)$	$\gamma^{K}_{0.6}$(MS14)	Δ^{K}_{ref}	Δ^{K}_{pro}
B03	0.62	0.66	0.60	0.03	0.05
IP13	0.41	0.53	0.50	0.11	0.01
Z09	0.28	0.48	0.54	0.25	0.04

Note. Δ^{K}_{ref} is the Difference between $\gamma^{K}_{0.6}(M^r_*)$ and $\gamma^{K}_{0.6}(M^V_*)$. Δ^{K}_{pro} is the Systematic bias in $\gamma^{K}_{0.6}$ Caused by the Minor Difference in Procedures between This Work and MS14.

difference in the procedures between this work and MS14 (Δ_{pro} in Table A1, as we already discussed in Section 6.4). This implies that assuming M_* from the same V band as the reference M_*, the recalibrated CMLRs in K band (on B–V color) based on the sample of LSBGs give very consistent $\gamma^{K}_{B--V=0.6}$ with those given by MS14 based on a sample of disk galaxies, which further indicates that there appears to be no apparent bias in $\gamma^{K}_{B--V=0.6}$ that was introduced by differences in samples between this work and MS14.

Compared with $\gamma^{K}_{B--V=0.6}(M^V_*)$, $\gamma^{K}_{B--V=0.6}(M^r_*)$ is 0.03, 0.11, and 0.25 dex lower by B03, IP13, and Z09. These offsets should only be caused by the difference in the assumption of reference M_* (M^r_* or M^V_*), so they were denoted as Δ_{ref} in Table A1 because these two sets of recalibrated relations only differ in the assumption of the reference M_*. This implies that different assumptions of reference M_* (M^r_* or M^V_*) would cause evident offsets in the $\gamma^{K}_{B--V=0.6}$ values predicted by recalibrated CMLRs. Quantitatively, M^r_*-based recalibrated CMLRs give $\gamma^{K}_{B--V=0.6}$ that are systematically lower by 0.03, 0.11, and 0.25 dex than those given by M^V_*-based recalibrated CMLRs (Table A1).

For the difference between $\gamma^{K}_{0.4}$ and $\gamma^{K}_{B--V=0.6}$ discussed in Section 6.4, $\gamma^{K}_{0.4}$ is 0.57, 0.42, and 0.30, and $\gamma^{K}_{B--V=0.6}$ is 0.60, 0.50, and 0.54 by B03, IP13 and Z09 after recalibration, and the difference between the two is 0.02, 0.08, and 0.26 dex for B03, IP13, and Z09 (Table 5). Numerically, the difference could be fully explained by the major offsets caused by the different assumptions of reference M_* ($\Delta_{ref} \sim 0.03$, 0.11, and

0.23 dex) and the minor offsets due to differences in the procedures between this work and MS14 ($\Delta_{\rm pro} \sim <0.05$ dex) (Table A1). This explanation should be plausible because $\gamma^K_{B--V=0.6}$ was predicted by MS14, who assumed M^V_* as the reference mass, while $\gamma^K_{0.4}$ was predicted by our recalibrated relations (Table 1), which assumed M^r_* as the reference mass. So considering the different assumptions of the reference M_* and the minor difference in the procedures between this work and MS14, the recalibrated CMLRs (B03, IP13, Z09) in the SDSS filters in this work (Table 1) are fundamentally consistent in γ^K_* at the equivalent colors with those in Johnson–Cousins filters by MS14.

In brief, the analysis in this Appendix demonstrate that compared with an assumption of M^V_* as the reference mass (MS14), the assumption of M^r_* as the reference mass (Section 5.2) would lower the self-consistent (also reference) M_* by 0.11, 0.25, and 0.33 dex, and lower γ^K_* by 0.03, 0.11, and 0.25 dex for B03, IP13, and Z09.

ORCID iDs

Wei Du https://orcid.org/0000-0003-4546-8216
Stacy S. McGaugh https://orcid.org/0000-0002-9762-0980

References

Abazajian, K. N., Adelman-McCarthy, J. K., Agüeros, M. A., et al. 2009, ApJS, 182, 543
Bell, E. F., & de Jong, R. S. 2001, ApJ, 550, 212
Bell, E. F., McIntosh, D. H., Katz, N., & Weinberg, M. D. 2003, ApJS, 149, 289, (B03)
Bertin, E., & Arnouts, S. 1996, A&AS, 117, 393
Chabrier, G. 2003, PASP, 115, 763
Courteau, S., Cappellari, M., de Jong, R., et al. 2014, RvMP, 86, 47
Du, W., Cheng, C., Wu, H., Zhu, M., & Wang, Y. G. 2019, MNRAS, 483, 1754
Du, W., Cheng, C., Zheng, Z., & Wu, H. 2020, AJ, 159, 138
Du, W., Wu, H., Lam, M. I., et al. 2015, AJ, 149, 199
Gallazzi, A., & Bell, E. F. 2009, ApJS, 185, 253
Girardi, L., & Bertelli, G. 1998, MNRAS, 300, 533
Girardi, L., Bertelli, G., Bressan, A., et al. 2002, A&A, 391, 195
Girardi, L., Bressan, A., Bertelli, G., & Chiosi, C. 2000, A&AS, 141, 371
Haynes, M. P., Giovanelli, R., Kent, B. R., et al. 2018, ApJ, 861, 49
Haynes, M. P., Giovanelli, R., Martin, A. M., et al. 2011, AJ, 142, 170
Herrmann, K. A., Hunter, D. A., Zhang, H. X., & Elmegreen, B. G. 2016, AJ, 152, 177
Into, T., & Portinari, L. 2013, MNRAS, 430, 2715, (IP13)
Kauffmann, G., Heckman, T. M., White, S. D., et al. 2003, MNRAS, 341, 33
Kroupa, P. 1998, in ASP Conf. Ser. 134, Brown Dwarfs and Extrasolar Planets, ed. R. Rebolo, E. L. Martin, & M. R. Zapatero Osorio (San Francisco, CA: ASP), 483
Lawrence, A., Warren, S. J., Almaini, O., et al. 2007, MNRAS, 379, 1599
Marigo, P., & Girardi, L. 2007, A&A, 469, 239
Marigo, P., Girardi, L., Bressan, A., et al. 2008, A&A, 482, 883
McGaugh, S. S., & Schombert, M. J. 2014, AJ, 148, 77, (MS14)
Portinari, L., Sommer-Larsen, J., & Tantalo, R. 2004, MNRAS, 347, 691
Roediger, J. C., & Courteau, S. 2015, MNRAS, 452, 3209, (RC15)
Schlafly, E. F., & Finkbeiner, D. P. 2011, ApJ, 737, 103
Schombert, J. M., & Rakos, K. 2009, AJ, 137, 528
Smith, J., Tucker, D., Kent, S., et al. 2002, AJ, 123, 2121
Taylor, E. N., Hopkins, A. M., Baldry, I. K., et al. 2011, MNRAS, 418, 1587
Zibetti, S., Charlot, S., & Rix, H.-W. 2009, MNRAS, 400, 1181, (Z09)